Electronic states of Cu(110) investigated with angle-resolved two-photon photoemission spectroscopy

Yasuyuki Sonoda*

The Institute of Physical and Chemical Research (RIKEN), 2-1 Hirosawa, Wako 351-0198, Japan

(Received 3 November 2010; revised manuscript received 21 March 2011; published 21 June 2011)

Occupied and unoccupied electronic states of Cu(110) were investigated with angle-resolved two-photon photoemission spectroscopy with an energy resolution of 30 meV. The high energy resolution enables the individual $n=1$ and 2 image-potential-derived structures to be distinguished. The $n=1$ structure was 0.85 eV below E_{vac} at $\bar{\Gamma}$. The effective mass of the electron for the structure was the same for both dispersions along the $\bar{\Gamma}\bar{X}$ and $\bar{\Gamma}\bar{Y}$directions within the experimental error. The $n=2$ structure appeared in the $L_{2'}$-L_1 gap along the $\bar{\Gamma}\bar{Y}$ direction, and it did not appear at $\bar{\Gamma}$, or along the $\bar{\Gamma}\bar{X}$ direction, which means that the $n=2$ structure was strongly affected by the bulk band. In this paper, other two-photon photoemission structures and dispersions are compared with results reported in the previous literature.

DOI: 10.1103/PhysRevB.83.245410 PACS number(s): 79.60.−i, 73.20.At

I. INTRODUCTION

Two-photon photoemission spectroscopy (2PPES) can be used to investigate both occupied and unoccupied electronic states to an energy resolution of 30 meV; its limitation comes from the bandwidth of short-pulse laser light. The energy resolution is an order of magnitude better than that of conventional inverse photoemission spectroscopy (IPES), which is several hundred meV.[1–16] The high energy resolution of 2PPES can be exploited to investigate the electronic states of the Cu(110) metal surface. 2PPES is a powerful way to study image-potential states. The image-potential states come from quantized electron waves repeatedly reflected between the crystal edge, where the energy is within the bulk band gap, and the surface-barrier potential. Single-crystal Cu surfaces of low indexes (100) and (111) and their vicinal faces have often been subjects of investigation,[17–32] whereas Cu(110) has hardly been investigated.[33] Surface-barrier-induced image-potential states cannot be present on the Cu(110) surface, because no bulk band gap exists between E_{vac} and $E_{vac}-0.85$ eV at $\bar{\Gamma}$. However, image-potential resonances, which hybridize with surface-truncated bulk states, are created when there is no bulk band gap. A calculation using the Green's function screened potential (GW) approximation of many-body perturbation theory predicts the existence of image resonances when there is no bulk band gap.[34] High-resolution experimental data on Cu(110) are needed to gain an understanding of the image-potential resonances. Moreover, there will be other 2PPE structures besides the image-potential-derived ones. The current study compares measured 2PPE spectra and dispersions with the results of IPES,[3–5,8–14,16] reflectance anisotropy spectroscopy (RAS),[2,35] scanning tunneling spectroscopy (STS),[36] angle-resolved photoemission spectroscopy (ARPES),[37–46] and other 2PPES measurements.[47–49]

II. EXPERIMENT

The experimental apparatus consisted of a titanium-sapphire laser with a 100 fs pulse width, an ultrahigh-vacuum (UHV) chamber system equipped with a hemispherical energy analyzer (Thermo VG, CLAM 4), and a He I discharge lamp. The base pressure was kept below 1.0×10^{-10} Torr. The output of the laser was frequency tripled into a photon energy range between 4.04 and 4.77 eV. The power was regulated to $\leqslant 0.1$ nJ/pulse by using a neutral density filter. The light was focused with a quartz lens of 350 mm focal length on a sample surface in the UHV chamber at an angle of 60° from the surface normal. The acceptance angle of the analyzer was set to ±3°. The energy resolution of the analyzer was better than 30 meV, as measured from the E_F feature of a Cu sample cooled to 30 K. The sample was biased by −1.0 V with respect to the chamber ground so that the low-energy cutoff of the spectrum gave the vacuum level of the sample. The Cu(110) surface was prepared by cycles of Ar^+ sputtering at room temperature (RT) and annealing to 700 K. Cleanliness was checked from the ultraviolet photoemission spectrum and low-energy electron diffraction pattern.

III. RESULTS

To identify the origin of the structures in the 2PPE spectra of Cu(110), the spectra were measured by using photon energies from 4.04 to 4.77 eV at $\bar{\Gamma}$ at RT (Fig. 1). Measuring with a photon energy of 4.77 eV enabled the available surface-parallel momentum $k_{||}$ to be extended. The photon energies of 2PPE experiments should not exceed the work function of the sample [4.52 eV for the Cu(110) surface], or else the photoemission intensities arising from the one-photon photoemission (1PPE) would be enormous. Setting the energy below the work function protects the detector of the analyzer and prevents deterioration of the energy resolution arising from the Coulomb interaction between electrons excited by the laser pulses. However, this limitation in turn restricts $k_{||}$ when the 2PPES is measured in an angle-resolved experiment. Hence, the current experiments use photon energies exceeding the work function at the expense of energy resolution, and the lower-energy portions of the spectra with photon energies of higher than 4.52 eV were not measured in order to avoid the photoemission from 1PPE (Fig. 1). Figure 1 shows occupied initial states ($2h\nu$ process), labeled d_α, d_β, and d_γ, unoccupied intermediate states ($1h\nu$ process), labeled B to E and S_1, and the unoccupied final state ($0h\nu$ process), labeled A. Structures A, C, S_1, and d_γ show a clear polarization dependence. Structure A is the final

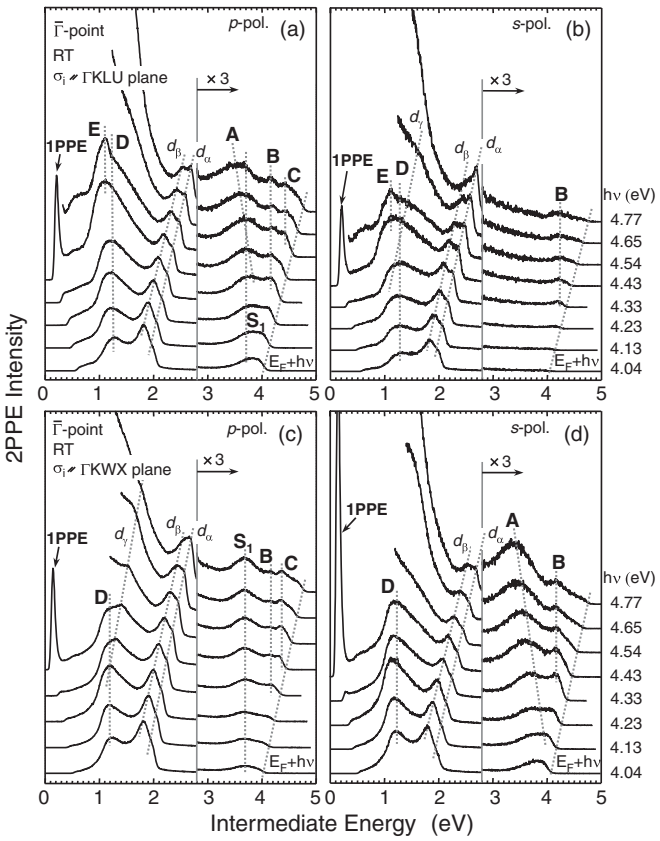

FIG. 1. 2PPE spectra of Cu(110) measured with a series of photon energies at $\bar{\Gamma}$ at RT. The incident planes σ_i of (a) and (b) are parallel to ΓKLU bulk mirror planes and those of (c) and (d) are parallel to ΓKWX. The polarizations of the incident light are indicated in each figure. The photon energies are shown at the right. 2PPE intensities are normalized to the peak of structure d_α in order to show all structures. The spectra are aligned to intermediate energy and are magnified by three times at above 2.8 eV after the intensity normalization. Right inclined, vertical, and left inclined dotted lines correspond to initial, intermediate, and final states in the 2PPE process, respectively.

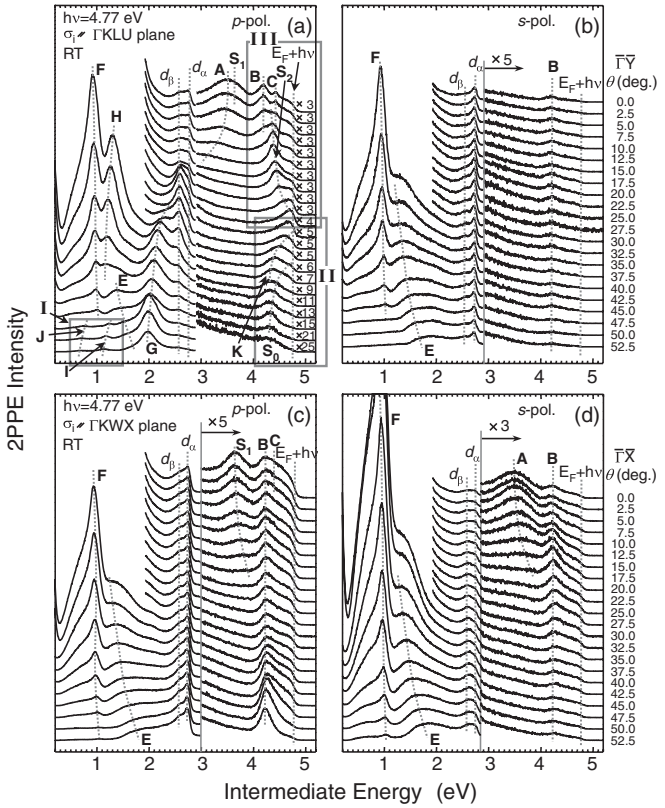

FIG. 2. Angle-resolved 2PPE spectra measured with the photon energy of 4.77 eV. (a)–(d) are the dispersions from the $\bar{\Gamma}$ point in Figs. 1(a)–1(d) along the $\bar{\Gamma}\bar{Y}$ and $\bar{\Gamma}\bar{X}$ directions of the surface Brillouin zone, respectively. The lower-energy portions of 2PPE spectra from $\theta = 0$ to 27.5° are not measured because of the dominant 1PPE components. The emission angle values from the surface normal are shown at the right. The spectra are magnified at above 2.9 eV. Dotted lines are guides for the eye. Portions of I to III are enlarged in Fig. 3.

state at 8.27 eV above E_F. In the *p*-polarization plot, structure *A* appears in the σ_i planes parallel to the ΓKLU plane, while it appears in the σ_i planes parallel to the ΓKWX plane in the *s*-polarization plot, where σ_i is the incident plane of the laser light. Structure *B* is an intermediate state at 4.22 eV above E_F, and it has no polarization dependence. Structures *C* and S_1 are intermediate states at 4.45 and 3.67 eV above E_F, respectively. Both structures appear only in the *p*-polarization plot in the σ_i planes parallel to the ΓKLU and ΓKWX planes. Structures *D* and *E* are the intermediate states at 1.24 and 1.05 eV above E_F, respectively. Structures d_α, d_β, and d_γ are the initial states at −2.04, −2.18, and −2.96 eV from E_F, respectively. Unlike d_α and d_β, d_γ appears in the σ_i planes parallel to the ΓKLU plane in the *s*-polarization plot and in the σ_i planes parallel to the ΓKWX plane in the *p*-polarization plot.

Figure 2 shows the angle-resolved 2PPE spectra measured with the photon energy of 4.77 eV at RT. The spectra show the dispersion features of the structures in Fig. 1. Structures labeled S_0, S_2, *G*, and *I* to *K* appear along the $\bar{\Gamma}\bar{Y}$ direction in the *p*-polarization plot but do not appear along the $\bar{\Gamma}\bar{X}$ direction. An extrapolation suggests that structures *E* and *F* persist even at $\bar{\Gamma}$(Fig. 9). Structure *A* disperses to a lower energy in the $\bar{\Gamma}\bar{Y}$ direction in the σ_i planes parallel to the ΓKLU plane in the *p*-polarization plot, whereas it disperses to a higher energy in the $\bar{\Gamma}\bar{X}$ direction in the σ_i planes parallel to the ΓKWX plane in the *s*-polarization plot. Structures *B*, d_α, and d_β show no dispersive features (see Fig. 9).

Figure 3 shows enlargements of the portions of Fig. 2(a) labeled I, II, and III. Structures *I* to *K* and S_0 in Figs. 3(a) and 3(b) disperse downward toward $\bar{Y}$ [see also Fig. 6(b)]. Structure S_2 in Fig. 3(c) does not appear at $\bar{\Gamma}$ but instead appears at angles of over 5.0° between the energies of structures *B* and *C*. The structure disperses upward in the $\bar{\Gamma}\bar{Y}$ direction. Structures *I* to *K*, S_0, and S_2 appear only in the *p*-polarization plot.

A surface state centered at $\bar{Y}$ at around 2 eV above E_F within the $L_{2'}$-L_1 gap observed in the angle-resolved IPES (ARIPES) studies disappeared when the sample was exposed to O_2.[8,11,13,14] In order to assess the surface sensitivity of structure *G* in Fig. 2(a), we conducted O_2 exposures from 0 to 20 L (0.5 monolayer adsorption at RT) for the purpose of confirming reproducibility. Figure 4 plots 2PPE spectra as

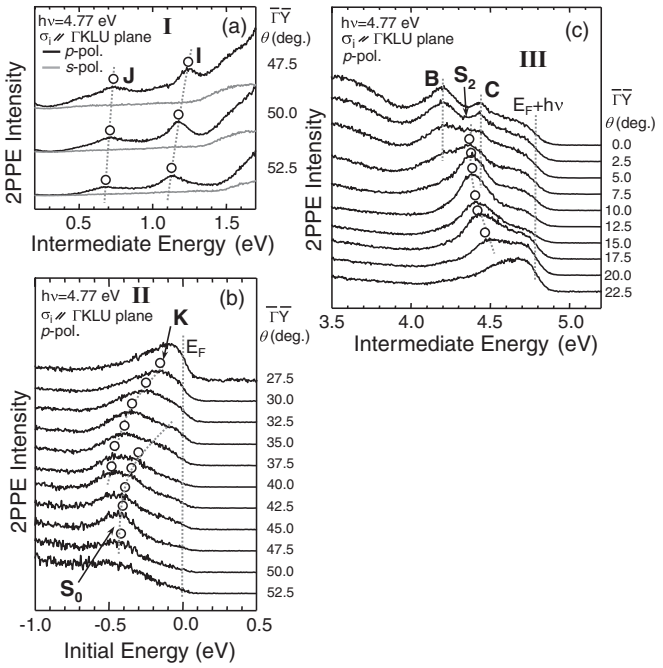

FIG. 3. (a)–(c) Enlargements of I, II, and III in Fig. 2(a). The spectra in (b) are plotted against the initial energy for convenience. Open circles correspond to those in Figs. 6(b) and 7(c).

a function of the amount of O_2 gas exposure at RT. After an exposure of 20 L, not only G but also E, F, H, and K completely disappear. These structures have considerable surface sensitivities. Structure D, which had been hidden before the O_2 exposure, appears after the other structures are quenched. It comes from a bulk band. Structures d_α and d_β persist even after 20 L of exposure.

Figures 5(a) and 5(b) plot the sample temperature dependence of the 2PPE intensities at a photon energy of 4.77 eV at $\bar{\Gamma}$. Figures 5(c) and 5(d) show the intensity changes of A, B, S_1, d_α, and d_β of Fig. 5(b) as a function of sample temperature. The intensities of d_α, d_β, and B monotonically increase with increasing sample temperature. In particular, B shifts to a lower

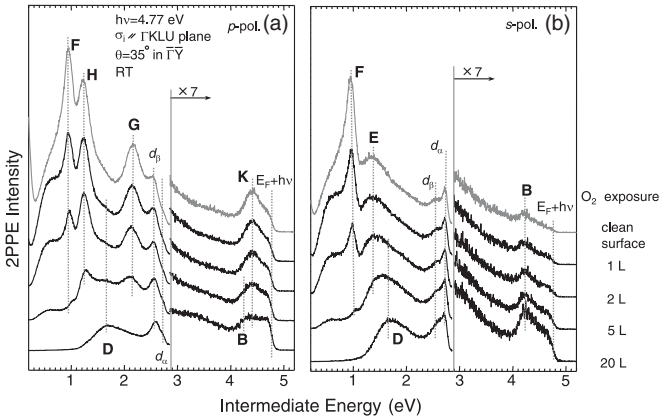

FIG. 4. 2PPE spectra measured with the photon energy of 4.77 eV at RT after O_2 exposure. (a) and (b) are at $\theta = 35^\circ$ along the $\bar{\Gamma}\bar{Y}$ direction in σ_i planes parallel to the ΓKLU plane (p- and s-polarizations, respectively). The amounts of O_2 are shown at the right. The spectra are magnified by seven times at above 2.9 eV.

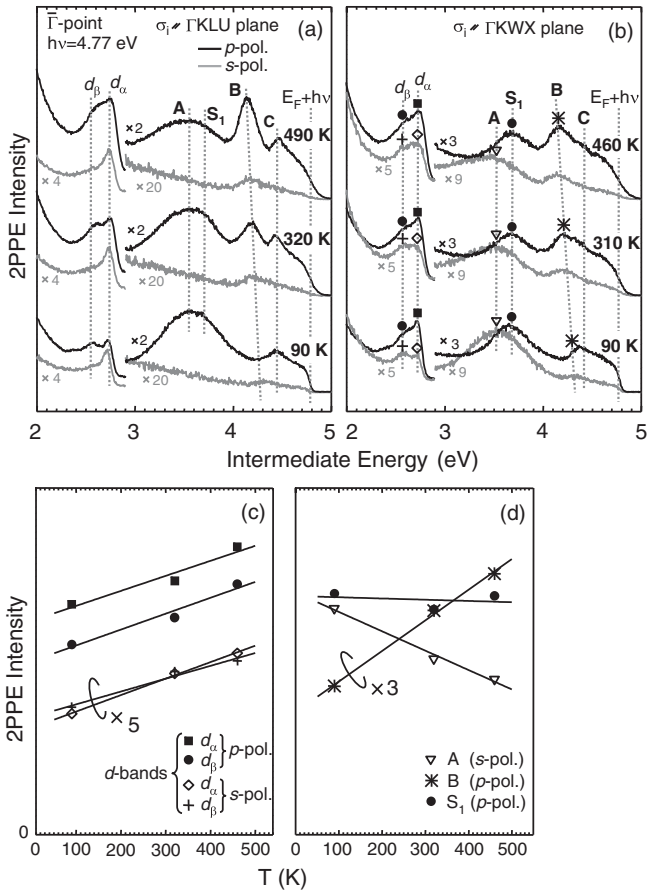

FIG. 5. The sample temperature dependence of 2PPE intensities measured with a photon energy of 4.77 eV. (a) and (b) are at $\bar{\Gamma}$ (p- and s-polarizations) in σ_i planes parallel to the ΓKLU and ΓKWX planes, respectively. The spectra are magnified at above 2.9 eV. The sample temperatures are shown at the right in each figure. (c) and (d) plot intensity changes with temperature of structures A, B, S_0, and d bands in (b). The intensities are directly taken from the peaks of structures in the experimental data. The lines in (c) and (d) are drawn straight for simplicity. The symbols in (b) correspond to those in (c) and (d).

energy with increasing temperature, as shown in Figs. 5(a) and 5(b). The sample temperature dependence of the energy of B is given by $E_m = 4.33$ eV–(0.38 meV/K)T. In contrast, the intensity of A decreases with increasing temperature. The intensities of S_1 are almost independent of the sample temperature.

Figure 6(a) illustrates the dispersive features of the S_0 structure from $\theta = 42.5^\circ$ to 52.5° along the $\bar{\Gamma}\bar{Y}$ direction with a photon energy of 4.33 eV in the p-polarization plot for the sake of comparison with Fig. 3(b) for the photon energy of 4.77 eV. Structures I to K and S_0 from the results of Figs. 3(a) and 3(b) together with structure S_0 from Fig. 6(a) are summarized on the projected bulk band structure of Cu(110) at around $\bar{Y}$ in Fig. 6(b).

In order to elucidate the dispersive features of S_1 at the photon energy of 4.33 eV, Fig. 7 shows angle-resolved 2PPE spectra from $\theta = 0$ to 25° at RT. Structure S_1 disperses upward along the $\bar{\Gamma}\bar{X}$ direction with the photon energy of 4.77 eV [Fig. 2(c)], whereas the dispersion is obscured by structure

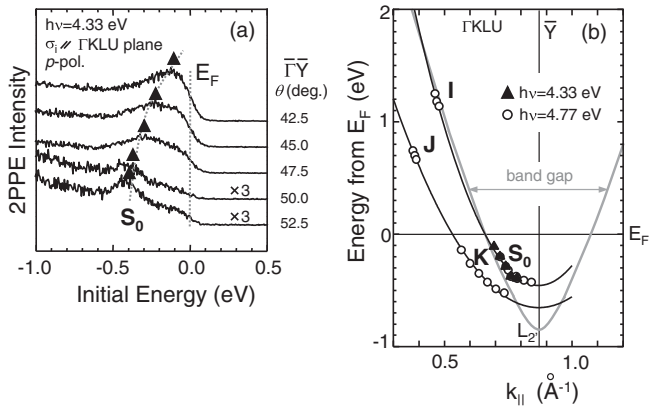

FIG. 6. (a) Dispersion of structure S_0 measured from $\theta = 42.5^\circ$ to 52.5° along the $\bar{\Gamma}\bar{Y}$ direction at a photon energy of 4.33 eV (p polarization) at RT. (b) Dispersion features of structures I to K and S_0 on schematic projected bulk band along the $\Gamma(^-)Y(^-)$ direction after Ref. 12. Open circles and closed triangles correspond to those in Figs. 3(a), 3(b), and 6(a).

A along the $\bar{\Gamma}\bar{Y}$ direction [Fig. 2(a)]. From Figs. 7(a) and 7(b), however, structure S_1 clearly shows dispersive features along the $\bar{\Gamma}\bar{X}$ and $\bar{\Gamma}\bar{Y}$ directions. Figure 7(c) summarizes the dispersions of S_1, from Figs. 2(c), 7(a), and 7(b), and S_2, from Fig. 3(c). The 2PPE intensity of S_1 rapidly decreases off $\bar{\Gamma}$ and completely disappears at $k_{||} = 0.3$ Å^{-1} along the $\bar{\Gamma}\bar{X}$ and $\bar{\Gamma}\bar{Y}$ directions. Structure S_2 appears only in the s-p band gap

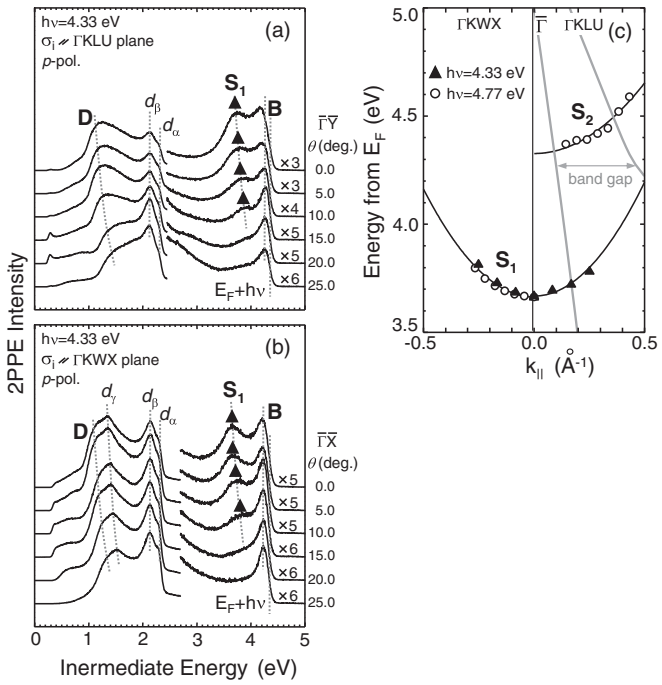

FIG. 7. Angle-resolved 2PPE spectra measured with the photon energy of 4.33 eV (p polarization) at RT. (a) and (b) are the dispersions from $\bar{\Gamma}$ in Figs. 1(a) and 1(c) along the $\bar{\Gamma}\bar{Y}$ and $\bar{\Gamma}\bar{X}$ directions of the surface Brillouin zone, respectively. The spectra are magnified at above 2.5 eV. (c) Dispersion features of structures S_1 and S_2 on schematic projected bulk bands along the $\Gamma(^-)X(^-)$ and $\Gamma(^-)Y(^-)$ directions after Ref. 12. Open circles and closed triangles correspond to those in Figs. 3(c), 7(a), and 7(b).

away from $\bar{\Gamma}$ along the $\bar{\Gamma}\bar{Y}$ direction. Figures 7(a) and 7(b) show the dispersive features of D and d_γ, whereas the features are hidden by structure E in Fig. 2 for the photon energy of 4.77 eV.

IV. DISCUSSION

A 2PPE experiment with the photon energy of 4.14 eV on the Cu(110) surface at $\bar{\Gamma}$ reported $n = 1$ and 2 image-potential resonances.[33] The energy of the $n = 1$ image-potential resonance was at 0.68 ± 0.1 eV below $E_{\rm vac}$, and the full width at half maximum, Γ_1, with a Lorentzian fitting of the resonance was 0.66 ± 0.06 eV. That $n = 1$ structure is comparable to S_1 at 0.85 eV below $E_{\rm vac}$ at $\bar{\Gamma}$, and the width Γ_1 of S_1 is 0.37 ± 0.01 eV with a Lorentzian fitting. Moreover, Γ_1 is rather similar to that of monolayer benzene on Cu(110) obtained with STS.[36] S_1 appears only in the p polarization [Figs. 1(a) and 1(c)]. The structure in Fig. 2(c) for the photon energy of 4.77 eV has an upward dispersion along the $\bar{\Gamma}\bar{X}$ direction. Although the dispersion of S_1 with the photon energy of 4.77 eV along the $\bar{\Gamma}\bar{Y}$ direction is not distinct because of the existence of structure A in the same energy region as in Fig. 2(a), the measurements with the photon energy of 4.33 eV clearly show dispersive features along the $\bar{\Gamma}\bar{Y}$ direction with a positive effective mass of $m^*/m = 1.81 \pm 0.20$ [Fig. 7(a)], where m^* is the effective mass of the electron, and m^*/m is determined from a parabolic fitting by taking $\bar{\Gamma}$ as the parabolic bottom. In Fig. 7(b), the structure disperses along the $\bar{\Gamma}\bar{X}$ direction with a positive effective mass of $m^*/m = 1.91 \pm 0.15$. The dispersive features in both directions are the same within the experimental error [Fig. 7(c)]. The dispersions along the $\bar{\Gamma}\bar{X}$ and $\bar{\Gamma}\bar{Y}$ directions have the same m^* as the $n = 1$ image-potential resonance although the surface lattice constants along the two directions are different (the surface lattice constant along $\bar{\Gamma}\bar{X}$ is 2.56 Å whereas the constant along $\bar{\Gamma}\bar{Y}$ is 3.61 Å). This indicates that the electron motion parallel to the surface is insensitive to the surface corrugation. ARPES studies on Cu(110) indicated that the $n = 1$ image "state" is along the $\bar{\Gamma}\bar{Y}$ direction, not along the $\bar{\Gamma}\bar{X}$ direction.[4,12] It was concluded that the image state is closely related to the projected bulk band gap in the ΓKLU plane. Within the interpretation of the one-dimensional two-band model, the gap is necessary for the appearance of image states.[12,50] However, a theoretical study using the GW approximation of many-body perturbation showed that image resonances exist as a result of hybridizing with surface-truncated bulk states even if there is no gap at those energies.[34] According to that study, the energy of the $n = 1$ image resonance for semi-infinite jellium with an aluminum density of $r_s = 2.07a_0$ was at -0.85 eV from $E_{\rm vac}$. Although the material is different from the current case, the energy of S_1 would be comparable. Time-resolved (TR) 2PPE experiments indicate that the population lifetimes τ_1 of the $n = 1$ states of Cu(100) and (111) surfaces are 35 ± 6 and 18 ± 5 fs, respectively.[25] τ_1 of S_1 is estimated to be 1.8 fs from $\Gamma_1 = \hbar/\tau_1 = 0.37$ eV, where Γ_1 and τ_1 are the linewidth and lifetime of the $n = 1$ state. Because of the hybridization with the bulk band, the lifetime of S_1 is over ten times shorter than those of the $n = 1$ states on the Cu(100) and (111) surfaces.

Structure S_2 does not exist at $\bar{\Gamma}$. It suddenly appears at $\theta = 7.5^\circ$, and its energy is between those of the B and C

structures. The structure disperses upward along the $\bar{\Gamma}\bar{Y}$ direction until $\theta = 20^\circ$ [Fig. 2(a) or 3(c)], at which point it disappears. Moreover, S_2 does not appear along the $\bar{\Gamma}\bar{X}$ direction. This means that the appearance of S_2 relates to the existence of the $L_{2'}$-L_1 gap [Fig. 7(c) or Fig. 9]. Extrapolation of the bottom of the parabolic dispersion of S_2 to $\bar{\Gamma}$ indicates that the bottom energy is at 4.33 eV above E_F and $m^*/m = 2.92$. The width Γ_2 with a Lorentzian fitting of S_2 at $\theta = 10^\circ$ is 0.24 eV, which is smaller than Γ_1. The characteristics of S_2 are entirely different from those of S_1 and resemble those of the $n = 1$ image state observed in the ARIPES studies.[4,12] However, the polarization dependence of S_2 is the same as that of S_1. The energy of S_2 extrapolated to $\bar{\Gamma}$ with a parabolic curve is at -0.19 eV from E_{vac}. The energies of the Rydberg-like image-potential states (resonances) are $E_n = -0.85/(n + a)^2$ eV from E_{vac},[12,26,50] where E_n is the energy of the nth state (resonance) and a is the quantum defect number. Since E_1 is at -0.85 eV from E_{vac}, a is 0.0 in this case. The energy of S_2 is close to that of the $n = 2$ Rydberg-like image state E_2, which is -0.21 eV from E_{vac}. The energy and polarization dependence would indicate that S_2 is the $n = 2$ Rydberg-like image state. The reason that S_1 and S_2 behave like the image resonance and state, respectively, may have to do with their phase continuity with the bulk bands. Structure C is observed in the p-polarization plot at 4.45 eV above E_F, which corresponds to -0.07 eV from E_{vac} at $\bar{\Gamma}$ (outside the $L_{2'}$-L_1 gap). Using again $E_n = -0.85/(n+0.0)^2$ eV, one finds that the energy of the $n = 3$ state is at -0.09 eV from E_{vac}. The polarization dependence and energy seem to indicate that structure C comes from the $n = 3$ image resonance. m^*/m was not estimated since the intensity of C was weak off the surface normal [Figs. 2(a) and 2(c)].

Regarding the other 2PPE structures, d_α and d_β show no dispersive features (Fig. 2 or Fig. 9). The energies are constant (-2.04 and -2.18 eV) from E_F to $k_\parallel$. In Ref. 47 2PPE spectra of Cs/Cu(100), (110), and (111) were measured with a photon energy of 3.08 eV at $\bar{\Gamma}$. These spectra had two d-band structures around -2.0 and -2.2 eV from E_F. The energies were almost independent of the surface indices, and they coincided with those of d_α and d_β in the measured spectra. The d-band structure at -2.0 eV from E_F in the plots of Ref. 47 was ascribed to a density of states (DOS) feature arising from an indirect transition through electron-phonon scattering from symmetry point X_5 to the sp band (band 6). Note that the band notation of the current paper matches those in Refs. 39 and 40. The fact that d_α is a nondispersive structure seems to indicate that it arises from an indirect transition process. The process might be related to a phonon-assisted transition, because the 2PPE intensity, as shown in Fig. 5(c), strongly depends on the sample temperature. The decoherence time T_2^{02} at -2.0 eV in the TR 2PPE experiments on Cs/Cu (110) and (111) also had a sample temperature dependence.[47] Moreover, the intensity of d_β increases with sample temperature, and its features resemble those of d_α. Thus, d_β seems to be a DOS feature originating from an indirect transition from a symmetry point that is energetically possibly, X_2 or L_3. Structure B appears at 4.22 eV above E_F at RT and has no polarization dependence. It shows no dispersive features (Fig. 2 or Fig. 9), and its intensity increases with sample temperature (Fig. 5). In the same manner as in the assignment of d_α and d_β, structure B can be ascribed to an indirect transition. However, the sample temperature dependence of the energy of B shows different features from those of d_α and d_β. B shifts to a lower energy, as shown in Fig. 5. Inspection of Cu's band structure shows that symmetry point L_1 at $\bar{\Gamma}$ of Cu(111) at 300 K is 4.25 eV above E_F, which is also the upper edge of the projected bulk band ($L_{2'}$-L_1) gap at point $\bar{Y}$ on the Cu(110) surface. The energy of B is close to the upper edge of the gap. The energy of L_1 decreases with increasing sample temperature through thermally induced lattice expansion.[51] The energy and temperature dependence of L_1 correspond to those of structure B. Thus, this structure is a DOS feature arising from an indirect transition from L_1 at point $\bar{Y}$. A Shockley-type state at -0.432 eV from E_F at 300 K at $\bar{Y}$ on Cu(110) was reported in an ARPES experiment.[38] The energy of the state has a sample temperature dependence in which E_0 linearly increases with the sample temperature T [$E_0 = -(0.510 \pm 0.015)$ eV+ $(0.26 \pm 0.02$ meV/K$)T$] through thermally induced lattice expansion. The constant of proportionality corresponds to that of B (-0.38 meV/K). The correspondence comes from the same bulk band gap at $\bar{Y}$.

At $\bar{\Gamma}$, structure A is the final state; it is 8.27 eV above E_F, and it has a specific polarization dependence. The structure appears only in the p-polarization plot in the σ_i planes parallel to the ΓKLU plane and appears only in the s-polarization plot in the σ_i planes parallel to the ΓKWX plane [Figs. 1(a) and 1(d), respectively]. This means that the dipole selection rule for the structure is satisfied when $\vec{E}$ is parallel to the $\langle 001 \rangle$ direction, where $\vec{E}$ is the electric field vector of the incident light. For the vertical momentum $k_\perp$ of structure A, the simple relation that $k_\perp$ is equal to $0.512 \times \sqrt{E_f + V_0}$ Å^{-1} is used in the manner of the free-electron final-state model, where E_f and V_0 are the final-state energy and the inner potential, respectively. The inner potential V_0 for Cu is set to -7.5 eV from E_F.[8] Since structure A is the final state, $k_\perp$ is 2.03 Å^{-1}, which corresponds to $0.83|\Gamma KX|$, where $|\Gamma KX|$ is the momentum (2.46 Å^{-1}) at the first Brillouin zone along the surface normal. From the Cu band structure[39,40] structure A can be ascribed to band 8, having Σ_1 symmetry as in Fig. 8, which shows the bulk band structure of Cu(110) normal to the surface. Taking account of the photon energies, one finds that the corresponding intermediate state is band 6, having Σ_3 symmetry.[8,43] From the dipole selection rule, only the optical transition from the Σ_3 to Σ_1 symmetry is allowed when the $\vec{E}$ is parallel to the $\langle 001 \rangle$ direction.[42,52] This condition is met by the polarization dependence of structure A. Thus, structure A must come from the direct transition from band 6 with Σ_3 symmetry (the intermediate state) to band 8 with Σ_1 symmetry (the final state in the bulk) as in Fig. 8. Structure A comes from the $0h\nu$ process of 2PPES on low-index clean Cu surfaces. With regard to the dispersion, structure A shows different dispersive features depending on whether the electron emission is in the $\bar{\Gamma}\bar{Y}$ or the $\bar{\Gamma}\bar{X}$ direction. Along the $\bar{\Gamma}\bar{Y}$ direction, structure A disperses downward with a negative effective mass of $m^*/m = -0.52$, and the parabolic bottom is taken to be $\bar{\Gamma}$. In contrast, the structure exhibits a positive effective mass of $m^*/m = 1.54$ along the $\bar{\Gamma}\bar{X}$ direction. The origin of this difference is not clear at this stage. In contrast to structures d_α and d_β, structure d_γ, which is at -2.96 eV from E_F at $\bar{\Gamma}$, appears only in the s-polarization plot in the σ_i

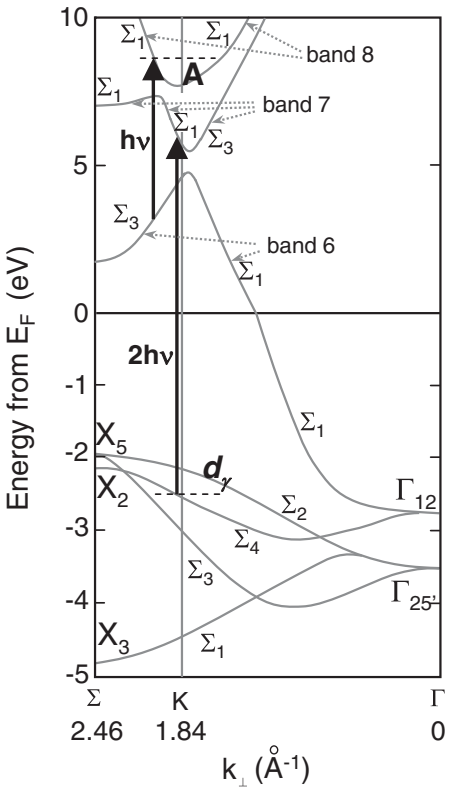

FIG. 8. Schematic bulk band structure along the surface normal of Cu(110) after Refs. 8, 39, 40, and 43. Upward arrows indicate the direct transitions of structures A and d_γ at $\theta = 0°$.

planes parallel to the ΓKLU plane and appears only in the p-polarization plot in the σ_i planes parallel to the ΓKWXplane, as Figs. 1(b) and 1(c) show. This means that this structure is observed when $\vec{E}$ is parallel to the $\langle 1\bar{1}0\rangle$ direction. Moreover, the structure disperses upward with a positive effective mass of $m^*/m = 1.92$ [Fig. 7(b)]. These characteristics indicate that d_γ is not from an indirect transition process like those at the origins of structures d_α and d_β. In the manner of the free-electron final-state model, we can estimate $k_\perp$ of structure d_γ for an excitation energy of 8.65 eV ($2h\nu$) in Fig. 7(b) to be 1.86 Å^{-1}, which corresponds to $0.76|\Gamma KX|$. Along the Σ symmetry line for Cu(110), the location of $k_\perp = 0.76|\Gamma KX|$ is around point K. The final state of d_γ is thus band 7 with Σ_1 symmetry (Fig. 8).[8,43] $2h\nu$ is equal to 8.65 eV in this case, and that makes the results of a PES study conducted at photon energies of 10 eV available for comparison.[45] According to the dipole selection rule, only the optical transition from the Σ_4 to Σ_1 symmetry is allowed when $\vec{E}$ is parallel to the $\langle 1\bar{1}0\rangle$ direction.[42,52] The polarization dependence of d_γ shows that the direct transition coherently occurs from d band Σ_4 (the initial state) to band 7 with Σ_1 symmetry (the final state) as in Fig. 8. Structure D was at 1.24 eV above E_F and had no polarization dependence (Fig. 1). This structure shows an upward dispersion in Figs. 7(a) and 7(b). A parabolic curve extrapolated to $\bar{\Gamma}$ and with $m^*/m = 1.67$ fits structure D. The dispersive features along the $\bar{\Gamma}\bar{X}$ direction are symmetric to those along the $\bar{\Gamma}\bar{Y}$direction. Structure D persisted even after 20 L of O_2 exposure, as Fig. 4(a) shows. These properties indicate that the structure comes from a direct transition in the bulk. ARIPES studies reported a bulk transition from bands 7,8→6 at around 1 eV above E_F.[8,11,13,16] From the dipole selection rule, structure D comes from a transition from band 6 having Σ_1 symmetry to band 8 having Σ_1 symmetry. $k_\perp$ of structure D is 1.85 Å^{-1} ($0.75|\Gamma KX|$) in the free-electron final-state model. However, band 6 at $k_\perp = 0.75|\Gamma KX|$ is around 5 eV above E_F (Fig. 8), which is different from the energy of structure D. There is a difference in energies between structure D and band 6.

In Fig. 2(a), structure G appears at angles above $\theta = 30°$ ($k_\parallel = 0.41$ Å^{-1}) along the $\bar{\Gamma}\bar{Y}$ direction. $k_\parallel$ at the energy at which structure G appears corresponds to the $L_{2'}$-L_1 gap edge or thereabouts. The structure is observed only in the p-polarization plots, and it disperses to lower energies from the gap edge toward $\bar{Y}$. Unfortunately, the features of G at $\bar{Y}$ cannot be accessed due to the limitation of $k_\parallel$. As in Fig. 4(a), the structure has strong surface sensitivity to O_2. These properties seem closely related to the surface state observed in the ARIPES studies at $\bar{Y}$ at around 2 eV above E_F.[5,8,11,13,14] That surface state showed a parabolic dispersion with $m^*/m = 0.8$, centered at $\bar{Y}$ at 1.8 eV above E_F.[12] The calculated ARIPE spectrum for the Cu(110) surface indicates that the components of the surface state are parallel to the surface normal.[5] Moreover, the surface state in the ARIPE spectra was sensitive to O_2 exposure.[8,11,13,14] Extrapolating the bottom of the parabolic dispersion of structure G to $\bar{Y}$ analogously to the case of ARIPES indicates that the bottom energy is at 1.81 eV above E_F and $m^*/m = 1.77$. Except for m^*/m, all of the surface-state characteristics in the ARIPES studies correspond to structure G. The RAS experiments show a surfacestate sensitive to oxygen exposure at 2.1 eV above

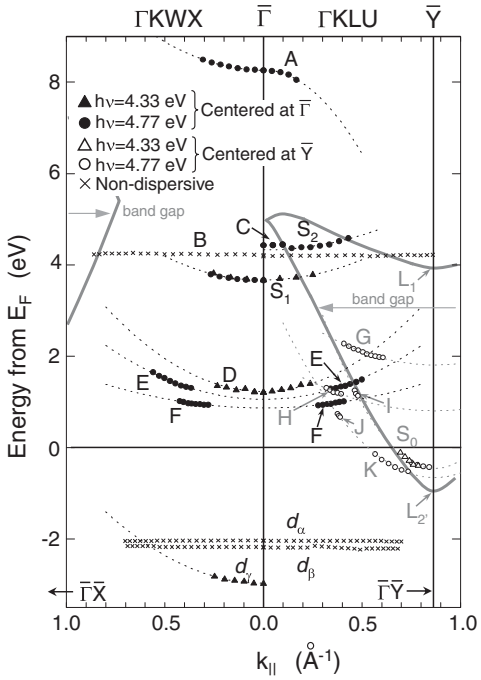

FIG. 9. Dispersion features in this study summarized in the schematic projected bulk bands along the $\bar{\Gamma}\bar{X}$ and $\bar{\Gamma}\bar{Y}$ directions after Ref. 12. Closed and open symbols indicate dispersion features centered at $\bar{\Gamma}$ and $\bar{Y}$, respectively, while crosses indicate nondispersive features.

TABLE I. Summary of 2PPE values derived from Figs. 1–7.

Label of structure	Parabolic center	m^*/m	$E - E_F$ (eV)	$E - E_F$ (eV) of references
A	$\bar{\Gamma}$	1.54 ($\bar{\Gamma}\bar{X}$), −0.52 ($\bar{\Gamma}\bar{Y}$)	8.27	8.9 (calc.)[a]
B	–	–	4.22	4.25 (calc.)[b]
C	$\bar{\Gamma}$	–	4.45(E_{vac}−0.07)	–
D	$\bar{\Gamma}$	1.67	1.24	4.9 (calc.)[a]
E	$\bar{\Gamma}$	2.08	1.05	–
F	$\bar{\Gamma}$	4.38	0.87	–
G	$\bar{Y}$	1.77	1.81	1.8 (expt.)[c]
H	$\bar{Y}$	1.68	0.62	–
J,K	$\bar{Y}$	0.67±0.01	−0.654	–
S_0,I	$\bar{Y}$	0.37±0.01	−0.462	−0.432 (expt.)[d]
S_1	$\bar{\Gamma}$	1.91±0.15 ($\bar{\Gamma}\bar{X}$), 1.81±0.20 ($\bar{\Gamma}\bar{Y}$)	3.67 (E_{vac}−0.85)	E_{vac}−0.68 (expt.)[e]
S_2	$\bar{\Gamma}$	−($\bar{\Gamma}\bar{X}$), 2.92 ($\bar{\Gamma}\bar{Y}$)	4.33 (E_{vac}−0.19)	E_{vac}−0.2 (expt.)[f]
d_α	–	–	−2.04	−2.01 (expt.)[g]
d_β	–	–	−2.18	−2.25 (expt.)[g]
d_γ	$\bar{\Gamma}$	1.92 ($\bar{\Gamma}\bar{X}$), −($\bar{\Gamma}\bar{Y}$)	−2.96	−2.65 (expt.)[h]

[a]Calculation values taken from Fig. 3 in Ref. 39.
[b]Calculation value from Table I in Ref. 51.
[c]Experimental value from Table II in Ref. 12.
[d]Experimental value from Table I in Ref. 38.
[e]Experimental value from Table I in Ref. 33.
[f]Experimental value taken from Fig. 5 in Ref. 33.
[g]Experimental values from Table I in Ref. 40.
[h]Experimental value from Table I in Ref. 45.

E_F.[2,35] With regard to structure H in Fig. 2(a), this structure resembles structure G, for example, in its polarization dependence, dispersion features, and oxygen exposure dependence. The main difference between the two structures is whether they appear within or outside the $L_{2'}$-L_1 gap. Structure H only appears outside the $L_{2'}$-L_1 gap, and the dispersion curve terminates at the band gap edge. Such behavior means that the structure is a surface resonance. Extrapolating the parabolic dispersion to $\bar{Y}$ shows that the bottom energy is 0.62 eV above E_F and $m^*/m = 1.68$. Although the ARIPES studies found surface states corresponding to structure G on Cu(110), Ag(110), and Ni(110) surfaces,[12] they did not find surface resonances corresponding to structure H.

The intensities of structures F and H gradually become smaller away from $\bar{\Gamma}$ and reach zero at angles above $\theta = 47.5°$ along the $\bar{\Gamma}\bar{Y}$ direction [Fig. 2(a)]. Instead of them, faint structures I and J appear [these structures are more visible in Fig. 3(a)]. Both structures were observed in the p-polarization plots and disperse toward lower energy with increasing θ. Structure S_0 observed in the p polarization disperses downward across the occupied Fermi edge at angles over $\theta = 35°$along the $\bar{\Gamma}\bar{Y}$ direction. The dispersion features are shown in detail in Fig. 3(b). Structure S_0 was also observed with the photon energy of 4.33 eV as shown in Fig. 6(a). The initial energy of S_0 does not vary with the photon energy ($2h\nu$ process). That means S_0 is an occupied state. Another structure K, which was also observed in the p-polarization plot, is on the lower-energy side of S_0. Structure K disperses in a similar way as S_0. The dispersion features of I to K and S_0 are plotted in Fig. 6(b), assuming K as the initial occupied state. The ARPES studies on Cu(110) reported a Shockley-type surface state around $\bar{Y}$.[38,41] The dispersion feature shows that the energy of the parabolic bottom near $\bar{Y}$ is −0.432 eV from E_F at RT, and $m^*/m = 0.26$.[38] Structures I and S_0 can be smoothly joined by a parabolic curve having a bottom at$\bar{Y}$, in analogy to the surface state in the ARPES studies; the bottom energy is −0.46 eV from E_F, and $m^*/m = 0.37 \pm 0.01$. Furthermore, the combined structures I and S_0 appear within the $L_{2'}$−L_1 gap. These features indicate that the structures come from a Shockley-type surface state, comparable with the ARPES results. This identification is appropriate if the polarization dependence is taken into account. The same can be done for I and S_0 and unoccupied J and occupied K by postulating that the parabolic bottom is at $\bar{Y}$ [Fig. 6(b)]. In contrast to structures I and S_0, J and K appear outside the $L_{2'}$−L_1 gap when the extrapolated bottom energy is −0.65 eV from E_F and $m^*/m = 0.67 \pm 0.01$. Since K is sensitive to O_2 exposure [Fig. 4(a)], J and K must come from surface resonances. Such an analogous surface resonance was reported in an ARIPES study on Ni(111).[53] The surface resonance on Ni(111) shows parabolic dispersion features outside the band gap edge from $\bar{\Gamma}$to $\bar{M}$.

As structures E and F in Fig. 2 are extrapolated to $\bar{\Gamma}$ with parabolic curves, these energies are at 1.05 and 0.87 eV above E_F with $m^*/m = 2.08$ and 4.38, respectively (Fig. 9). The dispersive features are symmetric along the $\bar{\Gamma}\bar{X}$ and $\bar{\Gamma}\bar{Y}$ directions. In particular, structure E appears at $\bar{\Gamma}$ with photon energies between 4.43 and 4.54 eV [Figs. 1(a) and 1(b)]. Structures E and F at $\theta = 35°$ along $\bar{\Gamma}\bar{Y}$ in the plot with the photon energy of 4.77 eV were perfectly quenched with 20 L pf O_2 exposure (Fig. 4). The surface sensitivities indicate that E and F come from surface resonances. The origin of these structures is different from that of structure D or the bulk band transition (bands 7,8→6) observed in the ARIPES experiments.[8,11,13,16]

Structures E and F appeared only as surface resonances in the 2PPE experiment, and a theoretical investigation of them must be undertaken before their origin can be assigned.

Figure 9 shows the dispersion features in the projected bulk band along the $\bar{\Gamma}\bar{X}$ and $\bar{\Gamma}\bar{Y}$ directions, and Table I summarizes the energies and the m^*/m of the 2PPE structures obtained by parabolic fitting.

V. CONCLUSIONS

The $n=1$ image-potential-derived structure S_1 was distinguished from the $n=2$ structure S_2 by exploiting the high energy resolution of 2PPES. The dispersions of the $n=1$ structure along the $\bar{\Gamma}\bar{X}$ and $\bar{\Gamma}\bar{Y}$ directions are symmetric (surface resonance), while the $n=2$ structure only appears in the $L_{2'}$-L_1 gap along the $\bar{\Gamma}\bar{Y}$ direction (surface state). Although the difference between the two structures as to their appearance in the Cu(110) band is not yet clear, the experimental results do shed light on the intrinsic difference between image-potential states and resonances. The faint structure C seems to be the $n=3$ image resonance.

The nondispersive structures d_α and d_β are assigned to the DOS of occupied d bands. The 2PPE intensities increase with the sample temperature due to phonon-assisted transitions. Structure B is the DOS of the upper edge of the projected bulk band ($L_{2'}$-L_1) gap at $\bar{Y}$. The energy of B shifts to a lower energy through lattice expansion as the sample temperature increases. The unoccupied A (band 8 in the $0h\nu$ process) and occupied d_γ (d band Σ_4 in the $2h\nu$ process) come from the direct transition satisfying the dipole selection rule. Those structures are observed when the $\vec{E}$ of the incident light is parallel to the $\langle 001\rangle$ and the $\langle 1\bar{1}0\rangle$ directions, respectively. Structure G is assigned to the surface state centered at $\bar{Y}$ within the $L_{2'}$-L_1 gap which was observed in the ARIPES studies, while structure H is assigned to the surface resonance centered at $\bar{Y}$ outside the $L_{2'}$-L_1 gap. Both structures are surface sensitive to oxygen exposure. The unoccupied I and occupied S_0 centered at $\bar{Y}$ come from Shockley-type surface state comparable with the ARPES results, while the unoccupied J and occupied K are assigned to the surface resonances centered at $\bar{Y}$. Structure D centered at $\bar{\Gamma}$ is an unoccupied bulk band, and structures E and F are assigned to surface resonances centered at $\bar{\Gamma}$. The high energy resolution is especially advantageous to investigate the unoccupied electronic states of Cu(110).

ACKNOWLEDGMENTS

The author thanks T. Munakata of Osaka University for fruitful discussions and help in conducting the experiment. This study was partially supported by Special Coordination Funds from the Ministry of Education Culture, Sports, Science and Technology of the Japanese Government.

*Present address: Toshiba Corporation; yasuyuki.sonoda@toshiba.co.jp

[1] O. Zeybek, A. M. Davarpanah, and S. D. Barrett, Solid State Commun. **138**, 290 (2006).
[2] O. Zeybek, A. M. Davarpanah, and S. D. Barrett, Surf. Sci. **600**, 5176 (2006).
[3] C. Su, D. Tang, and D. Heskett, Surf. Sci. **310**, 45 (1994).
[4] M. Grab, J. Braun, G. Borstel, R Schneider, H. Dürr, Th. Fauster, and V. Dose, J. Phys.: Condens. Matter **5**, 599 (1993).
[5] J. Redinger, P. Weinberger, H. Erschbaumer, R. Podloucky, C. L. Fu, and A. J. Freeman, Phys. Rev. B **44**, 8288 (1991).
[6] W. Altmann, K. Desinger, V. Dose, and A. Goldmann, Solid State Commun. **65**, 1411 (1988).
[7] R. Schneider, H. Dürr, Th. Fauster, and V. Dose, Phys. Rev. B **42**, 1638 (1990).
[8] W. Jacob, V. Dose, U. Kolac, Th. Fauster, and A. Goldmann, Z. Phys. B **63**, 459 (1986).
[9] R. A. Bartynski and T. Gustafsson, Phys. Rev. B **33**, 6588 (1986).
[10] D. Straub and F. J. Himpsel, Phys. Rev. B **33**, 2256 (1986).
[11] W. Jacob, V. Dose, and A. Goldmann, Appl. Phys. A **41**, 145 (1986).
[12] A. Goldmann, V. Dose, and G. Borstel, Phys. Rev. B **32**, 1971 (1985).
[13] B. Reihl and K. H. Frank, Phys. Rev. B **31**, 8282 (1985).
[14] R. A. Bartynski, T. Gustafsson, and P. Soven, Phys. Rev. B **31**, 4745 (1985).
[15] V. Dose, Surf. Sci. Rep. **5**, 337 (1985).
[16] W. Altmann, V. Dose, A. Goldmann, U. Kolac, and J. Rogozik, Phys. Rev. B **29**, 3015 (1984).
[17] M. Roth, Th. Fauster, and M. Weinelt, Appl. Phys. A **88**, 497 (2007).
[18] M. Rohleder, W. Berthold, J. Güdde, and U. Höfer, Appl. Phys. A **88**, 527 (2007).
[19] M. Hirschmann and Th. Fauster, Appl. Phys. A **88**, 547 (2007).
[20] Th. Fauster, M. Weinelt, and U. Höfer, Prog. Surf. Sci. **82**, 224 (2007).
[21] Th. Fauster and M. Weinelt, Surf. Sci. **593**, 1 (2005).
[22] P. M. Echenique, R. Berndt, E. V. Chulkov, Th. Fauster, A. Goldmann, and U. Höfer, Surf. Sci. Rep. **52**, 219 (2004).
[23] W. Berthold, P. Feulner, and U. Höfer, Surf. Sci. **548**, L13 (2004).
[24] M. Roth, M. Pickel, J. Wang, M. Weinelt, and Th. Fauster, Appl. Phys. B **74**, 661 (2002).
[25] M. Weinelt, J. Phys.: Condens. Matter **14**, R1099 (2002).
[26] Th. Fauster, Ch. Reub, I. L. Shumay, and M. Weinelt, Chem. Phys. **251**, 111 (2000).
[27] I. L. Shumay, U. Höfer, Ch. Reub, U. Thomann, W. Wallauer, and Th. Fauster, Phys. Rev. B **58**, 13974 (1998).
[28] H. Petek and S. Ogawa, Prog. Surf. Sci. **56**, 239 (1997).
[29] M. Wolf, Surf. Sci. **377–379**, 343 (1997).
[30] W. Wallauer and Th. Fauster, Surf. Sci. **374**, 44 (1997).
[31] T. Hertel, E. Knoesel, M. Wolf, and G. Ertl, Phys. Rev. Lett. **76**, 535 (1996).
[32] G. D. Kubiak, Surf. Sci. **201**, L475 (1988).
[33] B. Quiniou, V. Bulovic, and R. M. Osgood Jr., Phys. Rev. B **47**, 15890 (1993).
[34] G. Fratesi, G. P. Brivio, P. Rinke, and R. W. Godby, Phys. Rev. B **68**, 195404 (2003).

[35]K. Stahrenberg, Th. Herrmann, N. Esser, and W. Richter, Phys. Rev. B **61**, 3043 (2000).
[36]D. B. Dougherty, P. Maksymovych, J. Lee, and J. T. Yates Jr., Chem. Phys. Lett. **431**, 303 (2006).
[37]K. Berge, A. Gerlach, G. Meister, A. Goldmann, and E. Bertel, Phys. Rev. B **70**, 155303 (2004).
[38]P. Straube, F. Pforte, T. Michalke, K. Berge, A. Gerlach, and A. Goldmann, Phys. Rev. B **61**, 14072 (2000).
[39]W. Altmann, K. Dessinger, V. Dose, and A. Goldmann, Solid State Commun. **65**, 1411 (1988).
[40]R. Courths and S. Hüfner, Phys. Rep. **112**, 53 (1984).
[41]S. Kevan, Phys. Rev. B **28**, 4822 (1983).
[42]H. Przybylski, A. Baalmann, G. Borstel, and M. Neumann, Phys. Rev. B **27**, 6669 (1983).
[43]R. Courths, V. Bachelier, B. Cord, and S. Hüfner, Solid State Commun. **40**, 1059 (1981).
[44]P. Thiry, D. Chandesris, J. Lecante, C. Guillot, R. Pinchaux, and Y. Pétroff, Phys. Rev. Lett. **43**, 82 (1979).
[45]E. Dietz and F. J. Himpsel, Solid State Commun. **30**, 235 (1979).
[46]R. Courths, S. Hüfner, and H. Schulz, Z. Phys. B **35**, 107 (1979).
[47]H. Petek, H. Nagano, M. J. Weida, and S. Ogawa, Chem. Phys. **251**, 71 (2000).
[48]E. Knoesel, A. Hotzel, and M. Wolf, Phys. Rev. B **57**, 12812 (1998).
[49]S. Ogawa and H. Petek, Surf. Sci. **363**, 313 (1996).
[50]P. M. Echenique and J. B. Pendry, Prog. Surf. Sci. **32**, 111 (1990).
[51]R. Paniago, R. Matzdorf, G. Meister, and A. Goldmann, Surf. Sci. **336**, 113 (1995).
[52]J. Hermanson, Solid State Commun. **22**, 9 (1977).
[53]G. Borstel, G. Thörner, M. Donath, V. Dose, and A. Goldmann, Solid State Commun. **55**, 469 (1985).